Journal of Oceanography, Vol. 65, pp. 31 to 43, 2009

Subinertial and Seasonal Variations in the Soya Warm Current Revealed by HF Ocean Radars, Coastal Tide Gauges, and Bottom-Mounted ADCP

NAOTO EBUCHI*, YASUSHI FUKAMACHI, KAY I. OHSHIMA and MASAAKI WAKATSUCHI

Institute of Low Temperature Science, Hokkaido University, Kita-ku, Sapporo 060-0819, Japan

(Received 7 January 2008; in revised form 21 July 2008; accepted 22 July 2008)

Subinertial and seasonal variations in the Soya Warm Current (SWC) are investigated using data obtained by high frequency (HF) ocean radars, coastal tide gauges, and a bottom-mounted acoustic Doppler current profiler (ADCP). The HF radars clearly captured the seasonal variations in the surface current fields of the SWC. Almost the same seasonal cycle was repeated in the period from August 2003 to March 2007, although interannual variations were also discernible. In addition to the annual and interannual variations, the SWC exhibited subinertial variations with a period of 5–20 days. The surface transport by the SWC was significantly correlated with the sea level difference between the Sea of Japan and Sea of Okhotsk for both the seasonal and subinertial variations, indicating that the SWC is driven by the sea level difference between the two seas. The generation mechanism of the subinertial variation is discussed using wind data from the European Centre for Medium-range Weather Forecasts (ECMWF) analyses. The subinertial variations in the SWC were significantly correlated with the meridional wind stress component over the region. The subinertial variations in the sea level difference and surface current delay from the meridional wind stress variations by one or two days. Sea level difference through the strait caused by wind-generated coastally trapped waves (CTWs) along the east coast of Sakhalin and west coast of Hokkaido is considered to be a possible mechanism causing the subinertial variations in the SWC.

Keywords:
· Soya Warm Current,
· Sea of Okhotsk,
· coastal current,
· HF radar,
· coastally trapped wave.

1. Introduction

The Soya Warm Current (SWC) is a coastal boundary current that flows along the coast of Hokkaido into the Sea of Okhotsk (Fig. 1). The SWC flows into the Sea of Okhotsk from the Sea of Japan through the Soya/La Perouse Strait (referred to as the Soya Strait hereinafter), which is located between Hokkaido, Japan, and Sakhalin, Russia. It supplies warm, saline water from the Sea of Japan to the Sea of Okhotsk and greatly affects the ocean circulation and water mass formation in the Sea of Okhotsk, and local climate, environment and fisheries in the region. The volume transport by the SWC through the Soya Strait is also important in the mass budgets of the Seas of Japan and Okhotsk.

Since the SWC is dominated by a barotropic component (e.g., Aota, 1975, 1984; Matsuyama *et al*., 1999; Tanaka and Nakata, 1999), direct current measurement is needed in order to investigate the structure and variations of the SWC. However, the SWC has never been continuously monitored due to the difficulty of field observation, owing to severe weather conditions and sea ice coverage in winter, political issues at the border strait, and conflicts with intensive fishing activity. Most previous studies have been based on short-term or pointwise observations from moored current meters and shipboard acoustic Doppler current profilers (ADCPs) together with hydrographic surveys (e.g., Aota, 1975, 1984; Aota and Matsuyama, 1987; Matsuyama *et al*., 1999, 2006; Tanaka and Nakata, 1999; Ishizu *et al*., 2006). The detailed features of the SWC and its variations have not yet been revealed.

In order to continuously monitor the SWC in and around the Soya Strait, three high frequency (HF) radars were installed around the Strait (Fig. 1) in March 2003, and continuous observations started in August 2003. Ebuchi *et al*. (2006) analyzed the current data for the first year and reported that the radars clearly captured the spatial and temporal variations of the SWC in the region.

* Corresponding author. E-mail: ebuchi@lowtem.hokudai.ac.jp

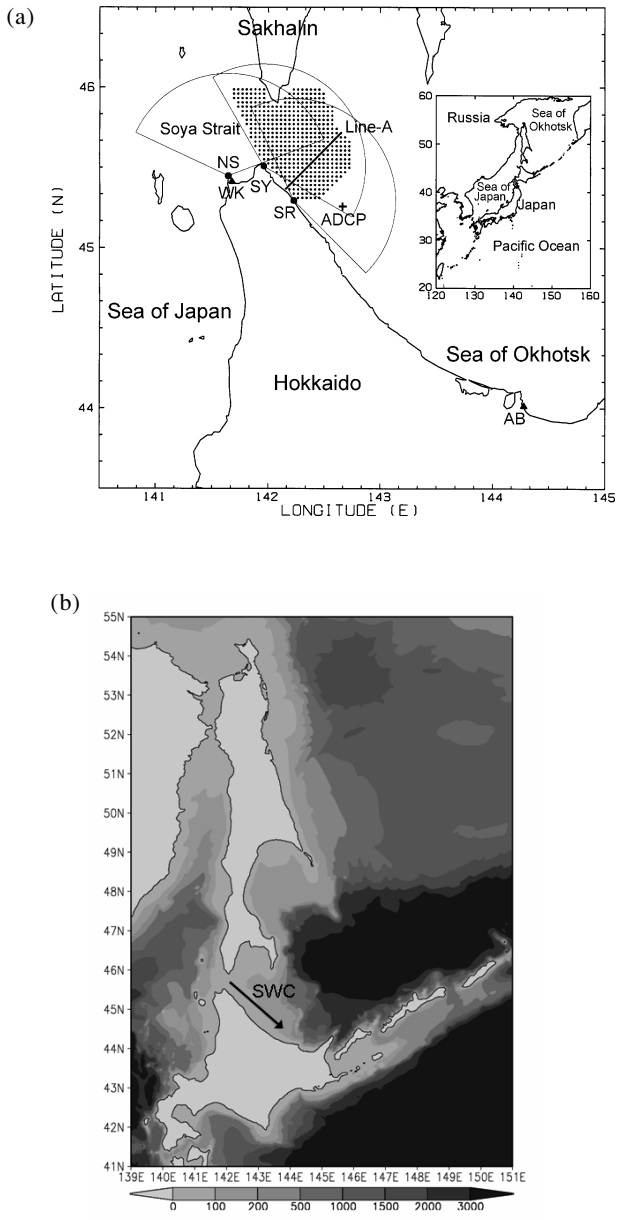

Fig. 1. (a) Map of the Soya/La Perouse Strait showing locations and coverage of the HF radar stations (NS: Noshappu, SY: Soya, SR: Sarufutsu), locations of the tide gauge stations (WK: Wakkanai, AB: Abashiri), and bottom-mounted ADCP (+), and (b) bathymetry of the Sea of Okhotsk based on the General Bathymetric Chart of the Oceans (GEBCO) data products (unit in meters). The dotted area in panel (a) shows typical coverage of the current vectors composed by data from the three HF radar stations. Line-A is the line where the surface velocity profile and transport are obtained. A conceptual path of the SWC is drawn in panel (b).

Fukamachi *et al*. (2008) estimated the volume transport of the SWC by combining the surface currents measured by the HF radars and vertical current profiles measured by a bottom-mounted ADCP. Although both of these studies used data for one year only, they demonstrated that the HF radar is a promising tool for revealing variations in the SWC.

In this paper we investigate subinertial, seasonal and interannual variations in the SWC by analyzing data obtained at these HF radar stations over a period of 44 months, from August 2003 to March 2007, together with coastal tide gauge records and current measurements by a bottom-mounted ADCP. We focus especially on the generation mechanism of the subinertial (5–20 days) variations in the SWC which are observed in the surface current and sea level data. Data used in the paper and data processing are described briefly in Section 2. Section 3 describes the seasonal evolution of the SWC and its interannual variations using the HF radar observations. Possible generation mechanisms of the subinertial variations in the SWC are discussed in Section 4. Finally, the paper is summarized in Section 5.

2. Data Processing

2.1 HF radar data

The three HF radar stations are located at Noshappu, Soya, and Sarufutsu (labeled as NS, SY and SR in Fig. 1(a)) in the vicinity of the Soya Strait. A SeaSonde HF-radar system (Barrick *et al*., 1977; Lipa and Barrick, 1983; Barrick and Lipa, 1997) manufactured by CODAR Ocean Sensors, Ltd. was used. The frequency of the radars is 13.9 MHz, and the range and azimuth resolutions are 3 km and 5°, respectively. The HF radars cover a range of approximately 70 km from the coast. The estimated coverage of the three radars is shown in Fig. 1(a). The observations were made hourly. We measured the beam pattern of the receiving antenna and corrected for the distortion of the antenna pattern to derive accurate radial velocities. Surface current vectors were composed in grid cells of 3 × 3 km (dots in Fig. 1(a)) using the radial velocity components observed by the radars according to a least squares method. Ebuchi *et al*. (2006) compared the hourly surface current velocities observed by the HF radars with in-situ data from drifting buoys and shipboard ADCPs. The current velocity derived from the HF radars agreed well with these data with root-mean-square (rms) differences less than 25 cm s^{-1}.

This study analyzes data obtained over a period of 44 months, from August 2003 to March 2007. In order to remove the tidal components, a 25-hour running average was applied to the time series of hourly surface current vectors in each grid cell, after which daily mean current fields were calculated. A 48-hour tide-killer filter (e.g.,

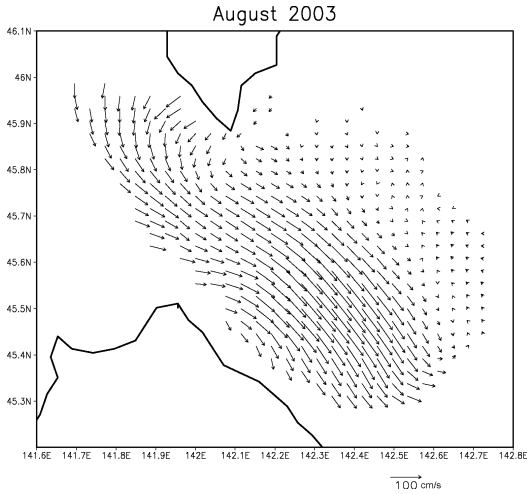

Fig. 2. Example of the monthly averaged surface current vector field after removing wind drift (August 2003).

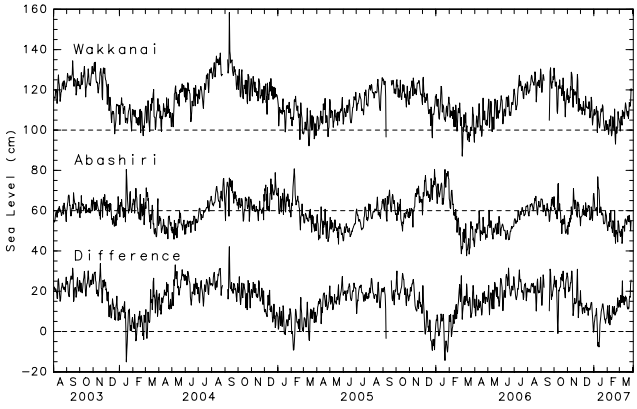

Fig. 3. Time series of the sea levels at Wakkanai and Abashiri and the difference between them (Wakkanai–Abashiri) from August 2003 to March 2007. For clarity the time series are drawn with a vertical shift, and dashed lines indicate zero, which is relative to T.P. (Tokyo Peil).

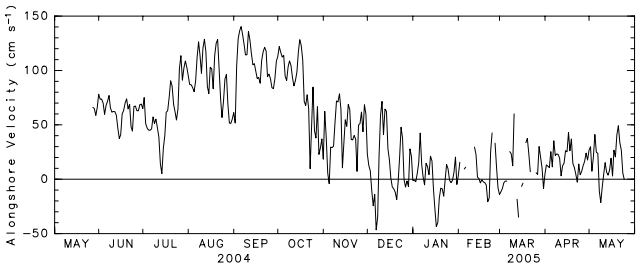

Fig. 4. Time series of the daily-averaged near-surface (9–13 m) velocity component in the southeastward direction observed by the bottom-mounted ADCP from May 2004 to May 2005.

Thompson, 1983; Hanawa and Mitsudera, 1985), which can eliminate tidal variations more precisely, was not utilized because there were several gaps in the surface current data. The daily means were not calculated at grid cells in which the number of hourly data points obtained was fewer than 15.

Since the velocity data obtained by HF radars contain wind drift, we attempt to remove this component using the daily nearby operational weather-forecasting wind data from the mesoscale grid point values (GPV) provided by the Japan Meteorological Agency. According to Fukamachi *et al*. (2008), the wind drift is estimated to be directed at 19.3° to the right of the wind and to have a speed reduction factor of 1.6%. These values of the angle and reduction factor were estimated by applying a least squares method to the relationship between daily nearby GPV wind data and the difference in daily velocities between the radar data ~25 km offshore and the uppermost (9–13 m depth) bottom-mounted ADCP data (Fukamachi *et al*., 2008). Using this angle and reduction factor, the daily wind-drift components were calculated from the daily wind data at nearby grid points and then removed from the original daily radar velocity.

Figure 2 shows an example of the monthly-averaged surface current fields (August 2003). The monthly surface current vector field clearly captures the SWC, which flows from west to east across the Soya Strait and turns southeastward along the coast. It also shows the southward current along the west coast of Sakhalin, as predicted by numerical experiments (Ohshima and Wakatsuchi, 1990; Ohshima, 1994). Zonal component of the surface velocity around Sakhalin might be overestimated, because the radial velocity components observed by the HF radars at outer ranges are noisier and the azimuth angle between the looking angles of the stations is narrow at these ranges.

2.2 Tide gauge records

Previous studies (e.g., Aota, 1975, 1984; Matsuyama *et al*., 1999; Ebuchi *et al*., 2006) reported that the surface velocity of the SWC is closely related to the sea level difference between the Seas of Japan and Okhotsk, since the SWC is considered to be driven by the sea level difference between these two seas (Aota, 1975, 1984; Ohshima, 1994; Lyu and Kim, 2005). In this study the sea level data from two tide gauge stations, Wakkanai (labeled WK in Fig. 1(a)) and Abashiri (AB in Fig. 1(a)), are used to represent the sea level variations in the Seas of Japan and Okhotsk, respectively. A 48-hour tide-killer filter developed by Hanawa and Mitsudera (1985) was applied to the hourly tide gauge records at these stations to eliminate the tidal variation precisely. The daily-mean sea levels were then calculated, and an atmospheric pres-

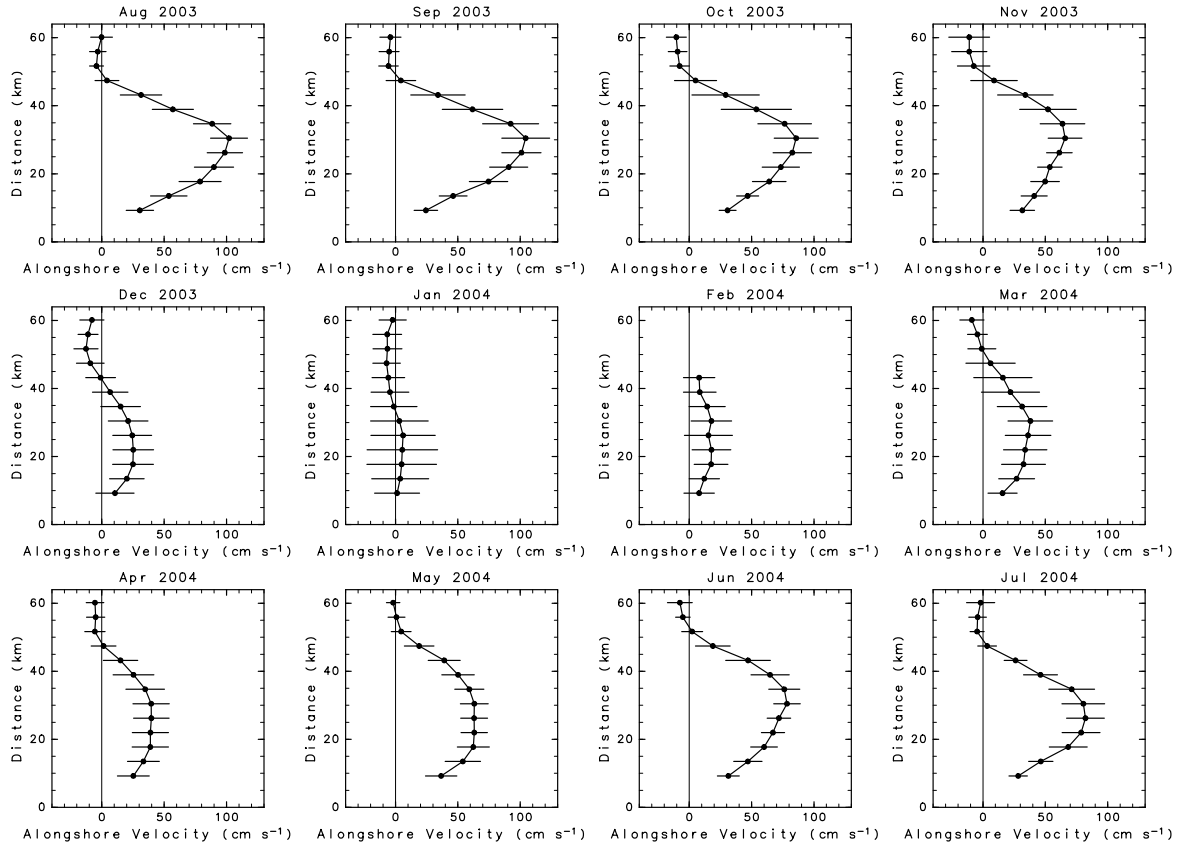

Fig. 5. Monthly-averaged profiles of the southeastward velocity component across Line-A (Fig. 1(a)) with respect to the distance from the coast from August 2003 to July 2004. Horizontal bars indicate the standard deviations calculated from daily-averaged velocity profiles.

sure correction was performed using the daily-mean sea level pressure observed at weather stations in Wakkanai and Abashiri. The time series at Wakkanai and Abashiri from August 2003 to March 2007 are shown in Fig. 3. The time series of the two tide gauge stations have been recorded since January 1968.

2.3 Bottom-mounted ADCP data

An ADCP (RD Instruments WH-Sentinel 300 kHz) was deployed 25 km off the coast of Hokkaido, where the water depth was approximately 90 m (Fig. 1(a)). The ADCP was housed in a trawl-resistant bottom mount (Flotation Technologies AL-200) to avoid damage from fishing activity. The measurement was carried out hourly from 25 May 2004 to 24 May 2005. The ADCP obtained valid data in nineteen 4-m bins from 81–85 m to 9–13 m. To remove the tidal components, a 25-hr running mean filter was applied to the data, after which daily average values were calculated. The daily-averaged, near-surface (9–13 m) velocity component in the direction of 154° (clockwise from north), which is the mean direction of the SWC at this point, was used in this study. The time series is shown in Fig. 4. Details of the ADCP observation and analyses of the current profile data were presented by Fukamachi *et al*. (2008). Although the time series of the near-surface currents observed by the ADCP was shorter than that of the radar data, the ADCP observations at 9–13 m depth were considerably less affected by wind drift than the surface currents observed by the HF radars.

2.4 Wind and wind stress fields

In Section 4 we present the relationship between variations in the SWC and the wind stress fields over the region. We utilized two sets of marine surface wind data from operational meteorological models of the European Centre for Medium-range Weather Forecasts (ECMWF). The ECMWF/WCRP level III-A Global Atmospheric (TOGA) Data Sets were used for the period from August 2003 to March 2007, which covers the observation period of the HF radars. The spatial resolution of the data sets is 2.5° × 2.5° and the temporal interval is 12 hours. The ECMWF Re-analysis (ERA-40) level III-B Global Atmospheric Data Archive was used for the period from January 1968 to August 2002. The spatial resolution of

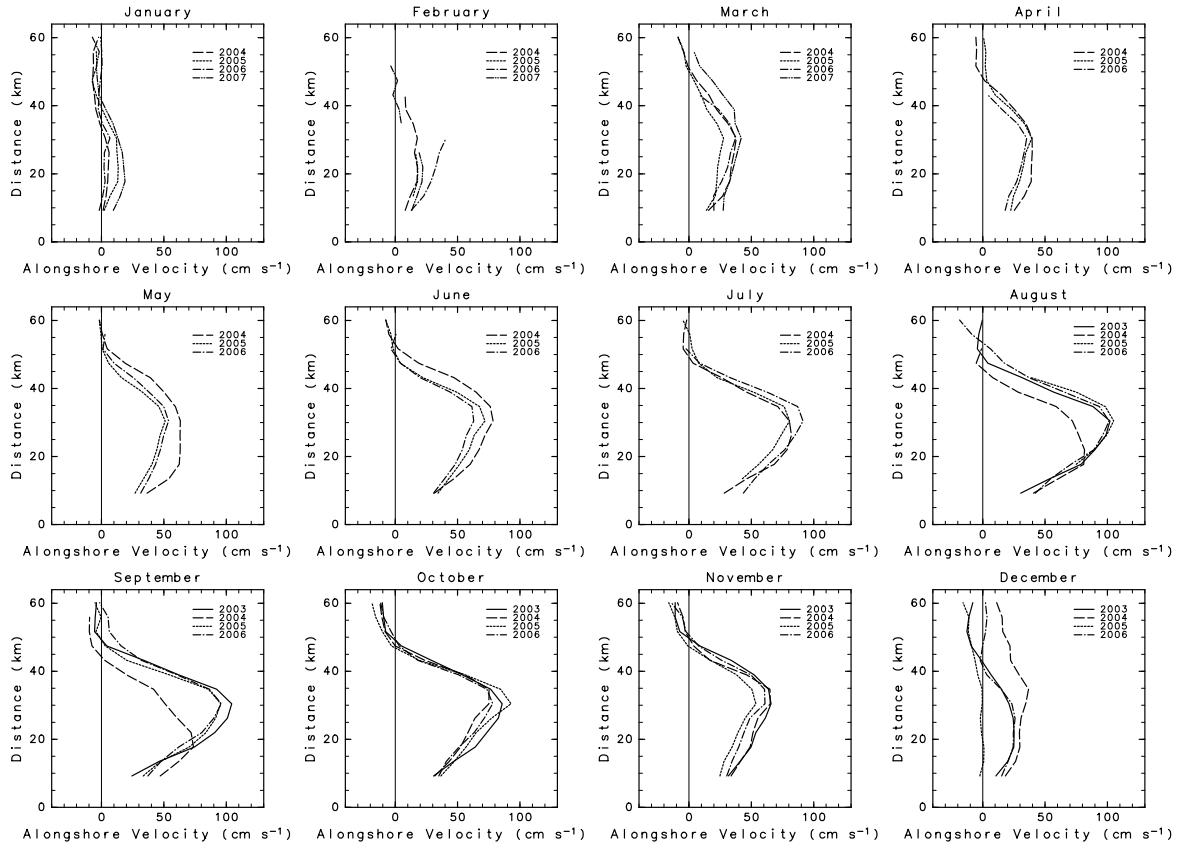

Fig. 6. Yearly variations of the monthly-averaged profiles of the southeastward current velocity component across Line-A.

the data set is 1.125° × 1.125° and the temporal interval is 6 hours. The ERA-40 was used for the analysis of the historical tide gauge records from 1968. The 10-m height wind velocity from the datasets was converted to the surface wind stress using the drag coefficient proposed by Smith (1988), ignoring the stability effects of the surface boundary layer and existence of sea ice. The wind stress was averaged daily at each grid cell and the daily-mean surface wind stress fields were used in this study.

3. Seasonal and Interannual Variations in the SWC

Daily southeastward current components across Line-A (Fig. 1(a)) were averaged monthly and are shown with standard deviations in Fig. 5 for the one-year period from August 2003 to July 2004. This line was selected since the surface current velocity of the SWC was strongest in this area (e.g., Fig. 2) and the data acquisition rate was relatively high. The monthly mean profiles show a clear seasonal variation. The velocity of the SWC reached a maximum of approximately 100 cm s^{-1} in summer (August and September) and became weak in winter (January and February). The current axis was located 20 to 40 km from the coast in this region, and the typical width of the SWC was approximately 50 km. These features of the SWC are consistent with the results of previous studies (Aota, 1984; Matsuyama *et al*., 1999). The standard deviations in summer and fall, when the SWC was strong, were smaller than those observed in winter, indicating the robust structure of the SWC in summer. No offshore data were obtained in February 2004 because of sea ice coverage.

Figure 6 shows year-to-year variations of the monthly-mean current profiles from August 2003 to March 2007. The almost identical seasonal cycle was repeated in these years, although some profiles indicated the presence of interannual variations. In 2004 the SWC was stronger in May and June than in other years, but weaker in August and September, when the locations of the velocity peak were closer to the coast. In December 2004 the southeastward velocity was stronger and extended farther offshore, compared to other years. In 2005 the SWC almost disappeared in December, despite having a velocity of 20–30 cm s^{-1} in December of other years.

Daily surface transport across Line-A was defined by integration of the daily southeastward current component along the line from the coast to a point at which the component becomes negative. If the current components were positive at all grid cells along the line, the integra-

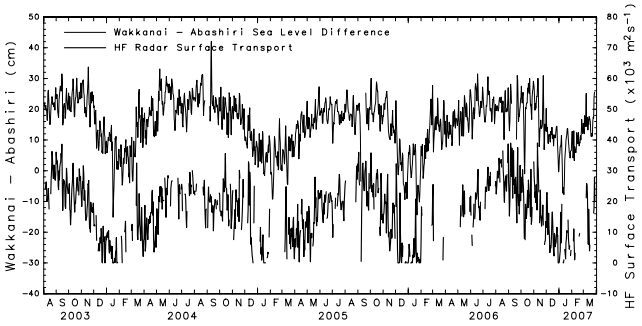

Fig. 7. Daily surface transport of the SWC (thick line) across Line-A and sea level difference between Wakkanai and Abashiri (thin line).

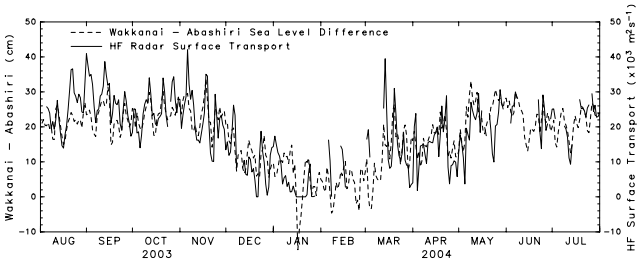

Fig. 8. Daily surface transport of the SWC (thin line) and sea level difference between Wakkanai and Abashiri (dashed line) for one year starting from August 2003.

tion was truncated at the farthest point (approximately 60 km from the coast). Figure 7 shows the time series of the surface transport (thick line). The surface transport also clearly shows seasonal variations in which the maximum surface transport occurred in summer to fall, and the minimum surface transport occurred in winter. The time series of the near-surface velocity observed by the bottom-mounted ADCP in Fig. 4 also shows similar seasonal variations.

The driving force of the SWC is ascribed to the sea level difference between the Seas of Japan and Okhotsk (Aota, 1975, 1984; Ohshima, 1994; Lyu and Kim, 2005). Most previous studies conventionally used the sea level difference between the Wakkanai (WK in Fig. 1(a)) and Abashiri (AB) tide gauge stations to represent the sea level difference between the two seas. A time series of sea level difference (same as in Fig. 3) is shown in Fig. 7 for comparison (thin line). The surface transport of the SWC and the sea level difference shows a good correlation with a correlation coefficient of 0.787. This result confirms that the SWC is driven by the sea level difference between the Seas of Japan and Okhotsk. Both time series also exhibit variations with time scales of approximately 10 to 15 days. These subinertial variations are discussed in the following section.

According to Figs. 6 and 7, it seems that interannual variations in the seasonal cycle of the SWC are not very significant. In Fig. 7 the sea level difference between Wakkanai and Abashiri, which is used to represent the intensity of the driving force of the SWC, shows similar seasonal cycles for the four years of the study. Under this condition, the structure of the SWC in this region, including the intensity of the current, location of the current axis, and shape of the horizontal velocity profile, did not change greatly, as shown in Fig. 6. This result might be interpreted in the light of the fact that the structure of the SWC in this region is controlled by the effects of bottom topography as coastal boundary current (Ohshima and Wakatsuchi, 1990). However, historical sea level records at these tide gauge stations show that the sea level difference between the Seas of Japan and Okhotsk varies significantly over interannual and decadal scales (e.g., Matsuyama *et al*., 1999; Minobe and Nakamura, 2004). Further studies using the longer time series of the current field data from HF radar and ADCP measurement are needed to clarify the interannual to decadal variations in the structure of the SWC.

Tsujino *et al*. (2008) investigated mechanisms governing the mean state and seasonal variation of the volume transports through the straits of the Sea of Japan using a simple analytical model and a basin-scale general circulation model. They simulated the seasonal variation of the volume transport through the Tsushima/Korea Strait, which is very similar to that observed by Takikawa *et al*. (2005). We believe that the seasonal variation of the volume transport through the Soya Strait and the mass budget of the Sea of Japan are of great interest. In this paper, however, we do not directly compare the observations by the HF radars with the results supplied by the models of Tsujino *et al*. (2008), because the HF radars only measure the surface velocity fields and cannot directly observe the volume transport of the SWC. In order to discuss relationships between the seasonal variations in the SWC and those of other straits, such as Tsushima/Korea, and, Tsugaru Straits, we have to estimate the volume transport accurately. Fukamachi *et al*. (2008) estimated the SWC volume transport by combing the vertical velocity profiles measured by a bottom-mounted ADCP with surface current fields derived from the HF radar system for one year only. However, the ADCP data are not available for the whole period of the HF radar observation. An ADCP observation campaign is now underway in this region, and we shall explore the seasonal variation in the SWC volume transport and its relationship with those in the other straits in the near future.

4. Subinertial Variations in the SWC

Figure 7 shows that subinertial variations exist in the

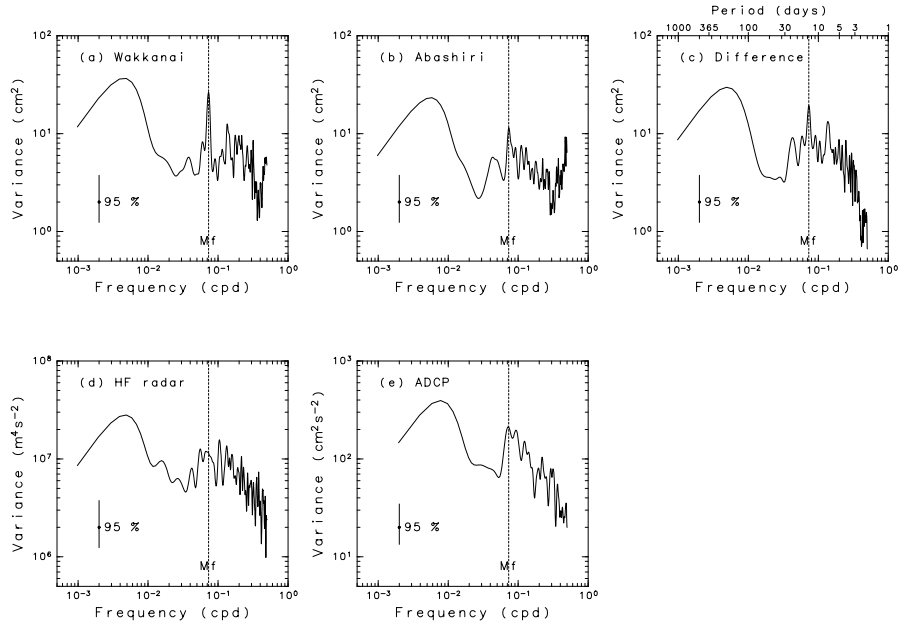

Fig. 9. Variance-preserving spectra of (a) the sea levels at Wakkanai and (b) Abashiri, (c) the sea level difference (Wakkanai–Abashiri), (d) the surface transport observed by the HF radars, and (e) the near-surface (9–13 m depth) velocity observed by the bottom-mounted ADCP. Unit of frequency is cycle per day (cpd). The frequency of the Mf tidal constituent is indicated by dashed lines. The 95% confidence limit is shown by a vertical bar.

SWC surface transport as well as the sea level difference along the Soya Strait with a temporal scale of approximately 10–15 days. Figure 8 is a close-up of Fig. 7 for the one-year period after August 2003. The surface transport and sea level difference oscillated coherently with a period of 10–15 days. These subinertial variations are also discernible in the near-surface current velocity observed with the bottom-mounted ADCP (Fig. 4). These velocity variations were observed from the surface to the bottom in the ADCP data, though the amplitude decreased slightly toward the bottom (data not shown here). Similar wintertime variations in the SWC were also reported by Aota and Kawamura (1978), although the generating mechanism of the variations was not clarified. In this section we explore possible generating mechanisms of the subinertial variations.

Figure 9 shows the variance-preserving spectra of the sea levels at (a) Wakkanai and (b) Abashiri, (c) the sea level difference (Wakkanai–Abashiri), (d) the surface transport observed by the HF radars, and (e) near-surface (9–13 m depth) velocity observed by the bottom-mounted ADCP. The spectra in panels (a)–(d) were calculated from the time series for 1024 days starting in August 2003, while the spectrum in panel (e) was calculated from the time series for 363 days from May 2004 with zero padding. Gaps in the time series were filled by linear interpolation. The mean and trend were removed from all the time series by fitting linear functions. Fast Fourier Transform (FFT) analysis was used to calculate the spectra. A Hanning filter was applied 20 times to smooth the spectra. The 95% confidence intervals were estimated according to Emery and Thomson (2001) and are shown in the figure.

In the spectra of the sea level difference (c), surface transport (d) and near-surface velocity (e), a broad peak at a frequency ranging from 5 to 20 days representing the subinertial variations can be discerned, together with a peak corresponding to the annual cycle. The period of the subinertial variations is longer than those of a Helmholtz resonance caused by atmospheric pressure variations (3–5 days, e.g., Lyu *et al*., 2002; Park and Watts, 2005), and of the shear instability of the SWC (1–3 days, Ohshima and Wakatsuchi, 1990).

Onishi *et al*. (2004) analyzed a time series of volume transport of the Tsugaru Warm Current observed by a shipboard ADCP and revealed a fortnightly oscillation. They inferred that the difference in the long-period lunar fortnightly (Mf) tide (13.66-day period) amplitude between the Sea of Japan and the North Pacific may have been responsible for the oscillation. The Mf tide is more energetic in the Sea of Japan, with an amplitude of 1–3 cm, while its amplitudes in the North Pacific and the Sea of Okhotsk are considerably smaller (Japan Coast Guard, 1992). A similar mechanism might cause the subinertial variations in the SWC, because it is driven by the sea level difference between the Seas of Japan and Okhotsk.

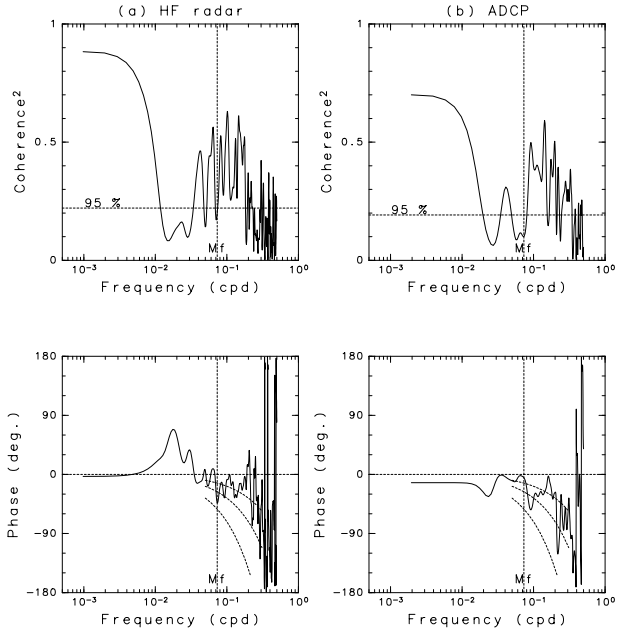

Fig. 10. Cross spectra of the sea level difference (Wakkanai–Abashiri) with (a) the HF radar surface transport and (b) ADCP near-surface velocity. Top and bottom panels show the squared-coherence and phase, respectively. Negative phase indicates that the sea level difference leads. The frequency of the Mf tidal constituent is indicated by vertical dashed lines, while horizontal dashed lines in upper panels represent the 95% confidence limit. Dashed curves in lower panels indicate phase lags (sea level leads) of 12 (upper), 24 (middle), and 48 (lower) hours, respectively.

In the spectrum of the sea level at Wakkanai (Fig. 9(a)) a sharp spike is discernible at the frequency of the Mf tide (dashed line), while the peak of the Mf tide is lower in the spectrum at Abashiri (Fig. 9(b)). This difference in the Mf tide amplitudes in the two seas caused a sharp peak at the Mf tide frequency in the spectrum of the sea level difference (Fig. 9(c)), as discussed by Onishi *et al*. (2004). In Figs. 9(d) and (e), however, the spectral peaks are broad and the energy is not concentrated at the Mf tide frequency.

Figure 10 shows cross spectra between the sea level difference and (a) the HF radar surface transport or (b) ADCP near-surface velocity. The spectral analysis was performed in the same way as for the power spectra shown in Fig. 9. Negative phase indicates that the sea level difference leads. In the frequency band of the subinertial variations around the period of 5–20 days (Fig. 9), the coherence between the sea level difference and the surface transport is generally high, as expected from the time series in Figs. 7 and 8. The coherence between the sea level difference and near-surface velocity is also high in the same frequency band. The sea level variations slightly lead the variations in the surface transport and near-surface velocity in this frequency range. However, the coherence at the Mf tide frequency is very low compared to those observed at the surrounding frequencies.

These results from the spectral analyses do not support the hypothesis that the subinertial variations in the SWC are caused by the difference between the Mf tide amplitudes in the Seas of Japan and Okhotsk. Although we consider the fact that the lengths of time series of the HF radar and bottom-mounted ADCP data are limited and acknowledge that several gaps in the time series have been filled by linear interpolation, the spectral peaks in Figs. 9(d) and (e) are considerably broader than those expected to be generated by the Mf tidal constituent. The coherence between the sea level difference and SWC surface transport or near-surface velocity at the Mf tide frequency is very low, as shown in Fig. 10. In Figs. 3(a) and (b) the subinertial variations are discernible not only in the sea level in Wakkanai but also in Abashiri, implying that the subinertial variations in the sea level difference in Fig. 3(c) are not generated solely by the contribution from the Sea of Japan, where the Mf tide amplitude is considerably larger than in the Sea of Okhotsk. Based on these results it is difficult to interpret all the subinertial variations in the SWC using only the Mf tide amplitude difference between the two seas, although the Mf tide is likely to contribute, at least partially, at a specific frequency.

Instead of the Mf tide amplitude difference, we examined the contribution of synoptic winds for the generation of subinertial variations in the SWC. Figure 11 shows the lag correlation between the ERA-40 wind stress fields and sea level difference (Wakkanai–Abashiri) for the period from January 1968 to August 2002. The azimuth direction of the wind stress component, which gives the maximum correlation with the sea level difference, is shown by the direction of the arrows, and the maximum correlation coefficient is denoted by the length of the arrows and contours. The maximum value of the correlation coefficient (0.564) is found in the vicinity of the Soya Strait with a one-day lag (middle panel), implying that the variations in the wind stress field lead those of the sea level difference by one day. The sea level difference is correlated with meridional wind stress, and southerly winds were observed to increase the sea level difference.

Given the result that the sea level difference between the Seas of Japan and Okhotsk is correlated with the meridional wind stress, we consider coastally trapped waves (CTWs) generated along the east and west coasts by the meridional wind as a possible mechanism causing the subinertial variations in the sea level difference and the velocity field of the SWC. Figure 12 shows a diagram of the mechanism. The coastlines of Sakhalin and Hokkaido are simplified to two meridional boxes (c.f., Fig. 1(b)).

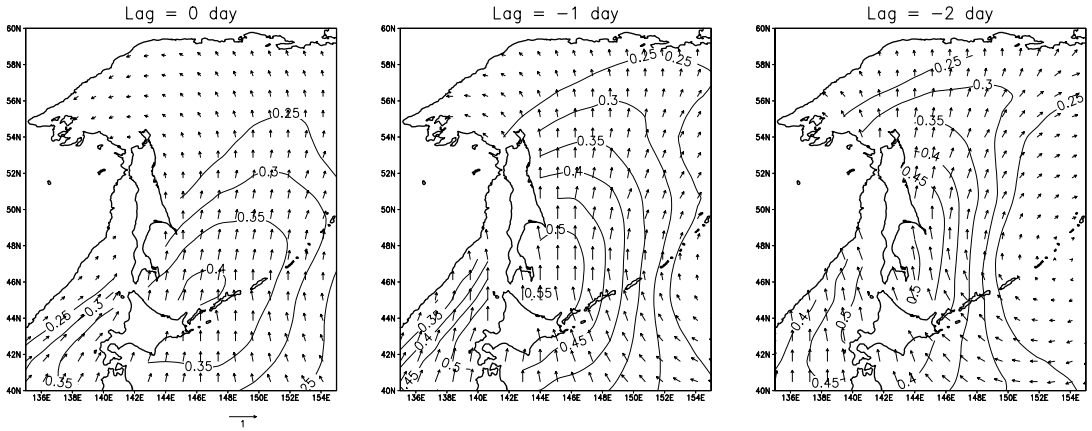

Fig. 11. Lag correlation between the ERA-40 wind stress fields and sea level difference (Wakkanai–Abashiri) from January 1968 to August 2002. The azimuth direction of the wind stress component, which gives the maximum correlation with the sea level difference, is shown by the direction of arrows, and the maximum correlation coefficient is shown by the length of arrows and contours. Negative lag time indicates that the wind stress field leads the sea level difference.

The Seas of Japan and Okhotsk, which are located west and east of the boxes, are connected by a narrow, shallow zonal strait (Soya Strait). Continental shelves extend along the coastlines west and east of the boxes. We assumed that a spatially uniform southerly wind blows over this region. The meridional wind generates CTWs propagating northward along the west coast and southward along the east coast (e.g., Gill and Schumann, 1974; Gill, 1982). In the case of the southerly wind, CTWs set up the sea level toward the coast in the Sea of Japan, whereas they decrease the sea level toward the coast in the Sea of Okhotsk. As a result, the sea level difference is enhanced by the CTWs propagating on both sides of the strait. Conversely, the sea level difference is reduced under the northerly wind. The sea level difference along the strait is believed to respond to the wind with some delay due to the propagation of the CTWs. Takeyama (2002) and Ishikawa (2007) presented similar ideas for interpreting the relationship between subinertial variations in the SWC and synoptic winds considering the effects of continental shelf waves.

The mechanism described above is qualitatively consistent with the results shown in Fig. 11. The variations in the sea level difference are thought to produce the subinertial variations in the current velocity of the SWC. Mizuta *et al*. (2005) analyzed long-term current measurements of the East Sakhalin Current off the east coast of Sakhalin Island and reported that the subinertial variations of the current velocity could be interpreted as CTWs generated by alongshore wind stress.

In order to confirm the relationship between the meridional wind and sea level difference, a cross spectrum between the ERA-40 meridional wind stress component and sea level difference was calculated for the

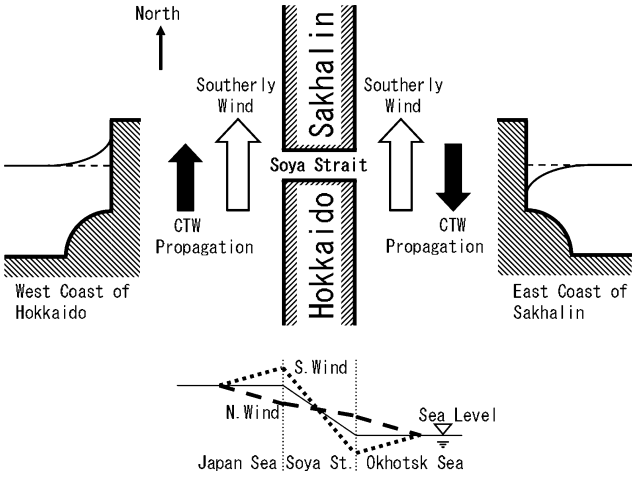

Fig. 12. Diagram of the generation mechanism of the subinertial variations in the SWC by wind-generated coastally trapped waves (CTWs).

period from January 1968 to August 2002. A grid cell located east of Sakhalin (47.25°N, 145.125°E) was selected for the ERA-40 wind stress to avoid the effects of land. Gaps in the time series of the sea level difference were filled by linear interpolation. The time series were divided into 12 segments with a length of 1024 days. The mean and trend were removed from all the samples of the time series by fitting linear functions. The FFT analysis was used to calculate the quadrature spectra. The 12 quadrature spectra were averaged and a Hanning filter was applied 4 times to smooth the spectra.

Figure 13 shows the (a) variance-preserving spectra of the ERA-40 meridional wind stress, (b) of the sea level

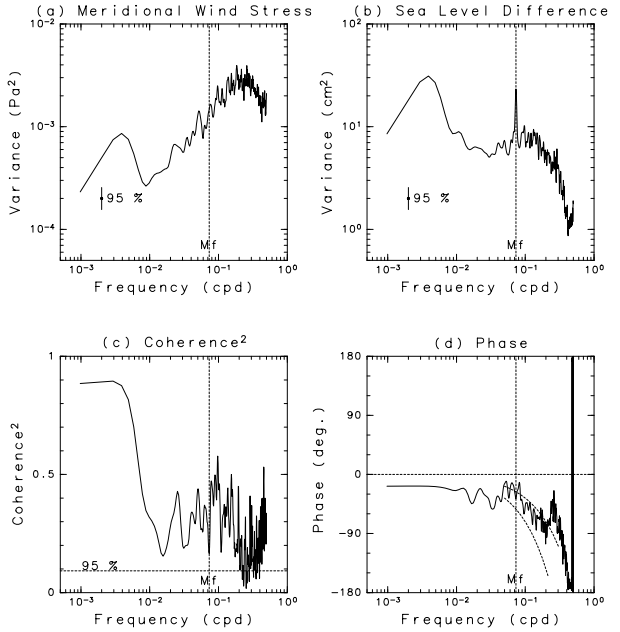

Fig. 13. Variance-preserving spectra of (a) the ERA-40 meridional wind stress at (47.25°N, 145.125°E) and (b) sea level difference (Wakkanai–Abashiri), and (c) the squared coherence and (d) the phase of the cross spectrum between them, calculated for the period from January 1968 to August 2002. Negative phase indicates that the meridional wind stress leads. The 95% confidence limit is indicated by a vertical bar in (a) and (b) and by a horizontal dashed line in (c). The frequency of the Mf tidal constituent is indicated by dashed vertical lines. Dashed curves in (d) indicate phase lags (wind leads) of one (upper) and two (lower) days, respectively.

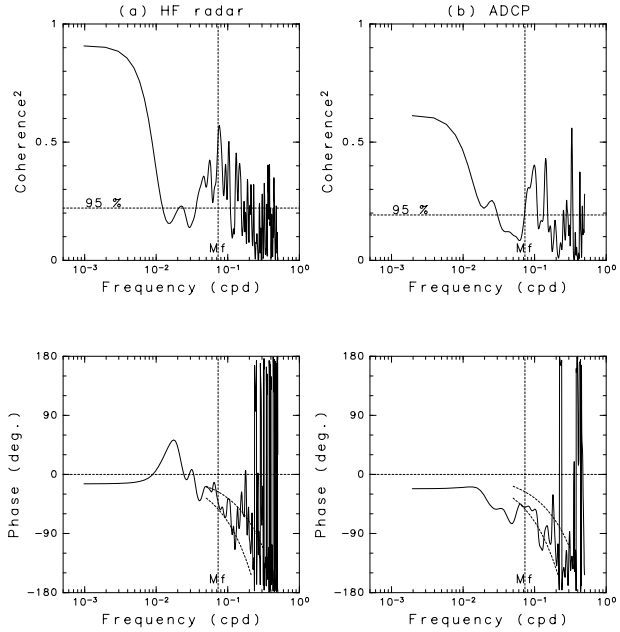

Fig. 14. Cross spectra of the ECMWF meridional wind stress at (47.5°N, 145.0°E) with (a) the HF radar surface transport and (b) ADCP near-surface current velocity. Top and bottom panels show the squared coherence and phase, respectively. Negative phase indicates that the meridional wind stress leads. The frequency of the Mf tidal constituent is indicated by dashed vertical lines, while the horizontal dashed lines in upper panels represent the 95% confidence limits. Dashed curves in the bottom panels indicate phase lags (wind leads) of one (upper) and two (lower) days, respectively.

difference, (c) the squared coherence, and (d) phase of the cross spectrum between them. The variance-preserving spectrum of the meridional wind stress has two peaks; one at lower frequency corresponds to the annual cycle, and the other at 3–5 day periods represents synoptic variations of the wind stress fields. As Fig. 9(c) also shows, the spectrum of the sea level difference exhibits a broad peak around the 5–20 day period with a sharp spike at the Mf tide frequency. The coherence also shows a broad peak in the frequency range of the subinertial variations. The phase indicates that the sea level difference was delayed by one to two days from the meridional wind stress variations in this frequency range (see the dashed curves in Fig. 13(d)). These results are consistent with those shown in Fig. 11 and support the mechanism in which the subinertial variations in the sea level difference are caused by the wind-generated CTWs, as depicted schematically in Fig. 12. In Figs. 13(a) and (b), the spectrum of the meridional wind stress has a peak around 5 days, while that of the sea level difference has a peak around 10 days. This difference in the peak periods implies that the response of the CTWs to the alongshore winds depends on the frequency. One can readily imagine that the CTWs are unable to respond to wind variations at very high frequency and that they may act as a low-pass filter (e.g., Gill and Schumann, 1974; Gill, 1982).

Cross spectra of the ECMWF meridional wind stress with the HF radar-derived surface transport and ADCP-derived near-surface current velocity were calculated using the wind stress data at one grid cell at (47.5°N, 145.0°E) and are shown in Fig. 14. The same procedure was used to calculate the cross spectra as those shown in Fig. 10. The result confirms that the surface transport and near-surface velocity of the SWC varied coherently with the meridional wind stress in the frequency range of 5–20 day periods, with a phase lag of one to two days (see the dashed curves in lower panels of Fig. 14). These results also support the generation mechanism of the subinertial variations described above.

Figure 15 shows the cross spectra between the ERA-40 meridional wind stress component and sea levels at

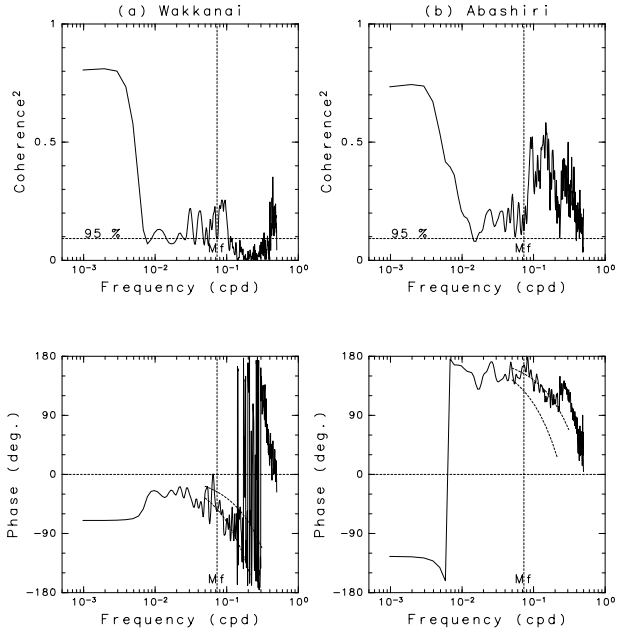

Fig. 15. Cross spectra of the ERA-40 meridional wind stress at (47.25°N, 145.125°E) with the sea levels at (a) Wakkanai, and (b) Abashiri. Top and bottom panels show the squared coherence and phase, respectively. Negative phase indicates that the meridional wind stress leads. The frequency of the Mf tidal constituent is indicated by dashed vertical lines, while the horizontal dashed lines in upper panels represent the 95% confidence limits. Dashed curves in the bottom panels indicate phase lags (wind leads) of one (upper) and two (lower) days, respectively.

(a) Wakkanai and (b) Abashiri, respectively. The same procedure was used to calculate the cross spectra as those for Fig. 13. The sea levels at both stations exhibit significant coherence with the meridional wind stress in the subinertial frequency range, although the coherence of the sea level at Abashiri is higher than that at Wakkanai. The coherence at Abashiri is higher in shorter periods (<10 days), while that at Wakkanai is higher in longer periods (>10 days). The phase relationship with the meridional wind stress is 180° opposed between Wakkanai and Abashiri, with time lags of one or two days from the wind stress in this frequency range. A positive meridional wind stress (i.e., southerly wind) generates a high sea level at Wakkanai and a low sea level at Abashiri with a lag of one or two days. This result also coincides with the schematic image in Fig. 12.

When the CTWs propagate along the east coast of Sakhalin and west coast of Hokkaido, the CTWs are expected to cause opposite anomalies in the sea levels along the both coasts, as depicted in Fig. 12. The sea levels at Wakkanai and Abashiri are expected to be out of phase in the subinertial frequency range. However, the cross spectrum between the sea levels at Wakkanai and Abashiri (not shown) showed neither significant coherence nor a 180° phase difference in the frequency range. We may interpret the results as follows. The anomaly in the sea level difference caused by the CTWs produces an anomaly in the current. By the geostrophic balance, the anomaly in the current sets up the sea level along the coast, which is in-phase in Wakkanai and Abashiri and tends to reduce the sea level difference caused by the CTWs. This adjustment might smear the coherence and phase relationship between the sea levels at Wakkanai and Abashiri.

Along the east coast of Sakhalin, Mizuta *et al*. (2005) clearly revealed the southward propagation of CTWs at subinertial frequencies (4 to 26 days) by analyzing long-term current measurements. Since we could not obtain sea level data along the east coast of Sakhalin and the number of tide gauge stations located in northern Hokkaido is very limited, we cannot exhibit the propagation of the CTWs using sea level data. From the results of Mizuta *et al*. (2005), however, it is reasonable to consider that sea level variations caused by the CTWs are dominant in the subinertial frequency range.

Several possible mechanisms have been proposed to explain how synoptic wind forcing over a narrow, shallow strait affects the volume transport through the strait. Lyu and Kim (2005) reported that the volume transport of the Tsushima Current through the Korea/Tsushima Strait is correlated with wind stress along the strait with a time scale of monthly periods, suggesting that the alongshore wind stress directly drives the strait flows. They estimated the effect of wind stress along the Soya Strait on the SWC volume transport to be one order of magnitude smaller than that of the Tsushima Current. Conversely, Jacobs *et al*. (2005) reported a correlation between the volume transport of the Tsushima Current and the wind stress across the strait in a synoptic frequency band (2–20 days), suggesting a Kelvin wave propagation as a possible mechanism. Ko *et al*. (2003) reported that observed current reversals at the Taiwan Strait could be explained by the combination of local wind stress over the strait and remote wind stress in the Yellow and East China Seas, the effect of which is provided by CTWs. The primary mechanism through which synoptic wind variation affects the current field and volume transport in a strait may depend on the shape of the coastlines and bathymetry surrounding the strait. The wind-generated CTWs, as proposed in this study, could be one of the possible physical mechanisms responsible for subinertial variations in a strait with straight coastlines with continental shelves, like the Soya Strait.

5. Summary and Concluding Remarks

Subinertial and seasonal variations in the SWC have

been investigated using data obtained by the HF ocean radars, coastal tide gauges, and a bottom-mounted ADCP. The HF radars clearly captured the seasonal variations in the surface current fields of the SWC. The velocity of the SWC reached its maximum, approximately 100 cm s^{-1}, in summer and fall, and became weaker in winter. The velocity core is located 20 to 30 km off the coast, and its width is approximately 50 km. A similar seasonal cycle was observed in the period from August 2003 to March 2007. Interannual variations were also discernible to some extent, although the time series analyzed in this paper are not long enough to discuss interannual variations in the SWC. In addition to the annual and interannual variations, the SWC exhibited subinertial variations with a period of 5–20 days. The surface transport by the SWC shows a significant correlation with the sea level difference between the Seas of Japan and Okhotsk as derived from the coastal tide gauge records at Wakkanai and Abashiri, for both seasonal and subinertial variations. These results indicate that the SWC is driven by the sea level difference between the two seas.

The generation mechanisms of the subinertial variations are here discussed using the surface transport estimated from the HF radar velocity fields, the near-surface current velocities observed by the ADCP, and the sea level difference between the Seas of Japan and Okhotsk derived from the coastal tide gauge records, together with wind data from the ECMWF analyses. The difference in the Mf tide amplitudes between the two seas may not be responsible for the subinertial variations, although Onishi *et al*. (2004) inferred that the fortnightly oscillations in the Tsugaru Warm Current may be caused by the difference between the Sea of Japan and the North Pacific. The differences of the shape of the coastlines and bathymetry in and around the Soya and Tsugaru Straits may be one of the reasons for the difference in generating mechanisms.

The results show that subinertial variations in the SWC are significantly correlated with the meridional wind stress component over the region. The subinertial variations in the sea level difference and surface current are delayed from the meridional wind stress variations by one or two days. We conclude that sea level difference through the strait caused by wind-generated CTWs on the east coast of Sakhalin and west coast of Hokkaido can be considered as a possible mechanism causing the subinertial variations in the SWC. Further studies using numerical models are needed to explore the physical mechanisms of the subinertial variations in the SWC in detail. As demonstrated by this study, the subinertial variations have a significant influence on the intensity of the SWC and are expected to have a marked impact on the marine environment and fisheries in this region. An understanding of the physical mechanisms is necessary for accurate prediction of the variations in the SWC.

Acknowledgements

The authors wish to express their gratitude to Yasushi Fujiyoshi, Kunio Shirasawa, Masao Ishikawa, and Toru Takatuska of the Institute of Low Temperature Science of Hokkaido University for their contribution to the operation of the HF radar system. They also thank Akira Masuda, Yutaka Yoshikawa, Kenji Marubayashi, and Michiyoshi Ishibashi of the Research Institute for Applied Mechanics (RIAM) of Kyushu University, Satoshi Fujii of University of the Ryukyus, and Akitugu Nadai of the National Institute of Information and Communications Technology (NICT) for their cooperation with respect to the design and construction of the HF radar system and stimulating discussions in meetings held under the RIAM Collaborative Research Program. Thanks are also extended to the captains and crew of the R/V Oyashio-maru and Hokuyo-maru, and Iori Tanaka, Hideo Yoshida, Shiro Takayanagi, and Tomohiro Ohtsuki of the Hokkaido Central and Wakkanai Fisheries Experimental Stations for their cooperation in the deployment and recovery of the bottom-mounted ADCP. The tide gauge records and meteorological data used in the present study were downloaded from the websites of the Japan Oceanographic Data Center (JODC) and Japan Meteorological Agency (JMA), respectively. The JMA GPV data were obtained from the website of the Research Institute for Sustainable Humanosphere, Kyoto University. Most figures in this paper were produced by the GFD-DENNOU Library and the Grid Analysis and Display System (GrADS). The present study was supported in part by Grants-in-Aid for Scientific Research (Nos. 17310002 and 18201002) from the Ministry of Education, Culture, Sports, Science and Technology (MEXT) of Japan.

References

Aota, M. (1975): Studies on the Soya Warm Current. *Low Temp. Sci., Ser. A*, **33**, 151–172 (in Japanese with English abstract).

Aota, M. (1984): Oceanographic structure of the Soya Warm Current. *Bull. Coast. Oceanogr.*, **22**, 30–39 (in Japanese).

Aota, M. and T. Kawamura (1978): Observation of oceanographic condition in the Okhotsk Sea coast of Hokkaido in winter. *Low Temp. Sci., Ser. A*, **37**, 93–105 (in Japanese with English abstract).

Aota, M. and M. Matsuyama (1987): Tidal current fluctuations in the Soya Current. *J. Oceanogr. Soc. Japan*, **43**, 276–282.

Barrick, D. E. and B. J. Lipa (1997): Evolution of bearing determination of HF current mapping radars. *Oceanography*, **10**, 72–75.

Barrick, D. E., M. W. Evans and B. L. Weber (1977): Ocean surface currents mapped by radar. *Science*, **198**, 138–144.

Ebuchi, N., Y. Fukamachi, K. I. Ohshima, K. Shirasawa, M. Ishikawa, T. Takatsuka, T. Daibo and M. Wakatsuchi (2006): Observation of the Soya Warm Current using HF ocean radar. *J. Oceanogr.*, **62**, 47–61.

Emery, W. J. and R. E. Thomson (2001): *Data Analysis Methods in Physical Oceanography (Second and Revised Edi-*

tion). Elsevier, Amsterdam, The Netherlands, 638 pp.
Fukamachi, Y., I. Tanaka, K. I. Ohshima, N. Ebuchi, G. Mizuta, H. Yoshida, S. Takayanagi and M. Wakatsuchi (2008): Volume transport of the Soya Warm Current revealed by bottom-mounted ADCP and ocean-radar measurement. *J. Oceanogr.*, **64**, 385–392.
Gill, A. E. (1982): *Atmosphere-Ocean Dynamics*. Academic Press, San Diego, California, U.S.A., 662 pp.
Gill, A. E. and E. H. Schumann (1974): The generation of long shelf waves by the wind. *J. Phys. Oceanogr.*, **4**, 83–90.
Hanawa, K. and H. Mitsudera (1985): On the data processing of daily mean values of oceanographic data.—Note on the daily mean sea-level data—. *Bull. Coast. Oceanogr.*, **23**, 79–87 (in Japanese).
Ishikawa, K. (2007): Variations of the Tsushima Warm Current system deduced from sea level differences across straits. Master's thesis of the Graduate School of Environmental Science, Hokkaido University, 35 pp. (in Japanese).
Ishizu, M., Y. Kitade and M. Matsuyama (2006): Formation mechanism of the cold-water belt formed off the Soya Warm Current. *J. Oceanogr.*, **62**, 457–471.
Jacobs, G. A., D. S. Ko, H. Ngodock, R. H. Preller and S. K. Riedlinger (2005): Synoptic forcing of the Korea Strait transport. *Deep-Sea Res. II*, **52**, 1490–1504.
Japan Coast Guard (1992): Tidal Harmonic Constants Tables, Japanese Coast. Hydrographic Publication, No. 742, 762 pp.
Ko, D. S., R. H. Preller, G. A. Jacobs, T. Y. Tang and S. F. Lin (2003): Transport reversals at Taiwan Strait during October and November 1999. *J. Geophys. Res.*, **108**(C11), 3370, doi:10.1029/2003JC001836.
Lipa, B. J. and D. E. Barrick (1983): Least-squares method for the extraction of surface currents from CODAR crossed-loop data: Applications at ARSLOE. *IEEE J. Ocean. Eng.*, **OE-8**, 226–253.
Lyu, S. J. and K. Kim (2005): Subinertial to interannual transport variations in the Korea Strait and their possible mechanisms. *J. Geophys. Res.*, **110**, C12016, doi:10.1029/2004JC002651.
Lyu, S. J., K. Kim and H. T. Perkins (2002): Atmospheric pressure-forced subinertial variations in the transport through the Korea Strait. *Geophys. Res. Lett.*, **29**(9), 1294, doi:10.1029/2001GL014366.
Matsuyama, M., M. Aota, I. Ogasawara and S. Matsuyama (1999): Seasonal variation of Soya Current. *Umi no Kenkyu*, **8**, 333–338 (in Japanese with English abstract and figure captions).
Matsuyama, M., M. Wadaka, T. Abe, M. Aota and Y. Koike (2006): Current structure and volume transport of the Soya Warm Current in summer. *J. Oceanogr.*, **62**, 197–205.
Minobe, S. and M. Nakamura (2004): Interannual to decadal variability in the southern Okhotsk Sea based on a new gridded upper water temperature data set. *J. Geophys. Res.*, **109**, C09S05, doi:10.1029/2003JC001916.
Mizuta, G., K. I. Ohshima, Y. Fukamachi and M. Wakatsuchi (2005): The variability of the East Sakhalin Current induced by winds over the continental shelf and slope. *J. Mar. Res.*, **63**, 1017–1039.
Ohshima, K. I. (1994): The flow system in the Japan Sea caused by a sea level difference through shallow straits. *J. Geophys. Res.*, **99**, 9925–9940.
Ohshima, K. I. and M. Wakatsuchi (1990): A numerical study of barotropic instability associated with the Soya Warm Current in the Sea of Okhotsk. *J. Phys. Oceanogr.*, **20**, 570–584.
Onishi, M., Y. Isoda, H. Kuroda, M. Iwahashi, C. Satoh, T. Nakayama, T. Ito, K. Iseda, K. Nishizawa, S. Shima and O. Togawa (2004): Winter transport and tidal current in the Tsugaru Strait. *Bull. Fish. Sci. Hokkaido Univ.*, **55**, 105–119.
Park, J.-H. and D. R. Watts (2005): Response of the southwestern Japan/East Sea to atmospheric pressure. *Deep-Sea Res.*, **52**, 1671–1683.
Smith, S. D. (1988): Coefficients for sea surface wind stress, heat flux and wind profiles as a function of wind speed and temperature. *J. Geophys. Res.*, **93**, 15,467–15,472.
Takeyama, Y. (2002): Variation of the Soya Warm Current in winter. Master's thesis of the Graduate School of Environmental Earth Science, Hokkaido University, 75 pp. (in Japanese).
Takikawa, T., J.-H. Yoon and K.-D. Cho (2005): The Tsushima Warm Current through Tsushima Straits estimated from ferryboat ADCP data. *J. Phys. Oceanogr.*, **35**, 1154–1168.
Tanaka, I. and A. Nakata (1999): Results of direct current measurement in the La Perouse Strait (the Soya Strait), 1995–1998. *PICES Sci. Rep.*, **12**, 173–176.
Thompson, R. O. R. Y. (1983): Low-pass filters to suppress inertial and tidal frequencies. *J. Phys. Oceanogr.*, **13**, 1077–1083.
Tsujino, H., H. Nakano and T. Motoi (2008): Mechanism of currents through the straits of the Japan Sea: mean state and seasonal variation. *J. Oceanogr.*, **64**, 141–161.